EPSC Abstracts
Vol. 8, EPSC2013-866, 2013
European Planetary Science Congress 2013

Constraints on Mars' recent equatorial wind regimes from comparison of observed with GCM-predicted aeolian feature orientations

E. Sefton-Nash (1), N. A. Teanby (2), C. Newman (3), R. A. Clancy (2) and M. I. Richardson (3)
(1) Department of Earth and Space Sciences, University of California Los Angeles, 595 Charles Young Drive East, Box 951567, Los Angeles, CA 90095-1567, USA (esn@ucla.edu).
(2) School of Earth Sciences, University of Bristol, Wills Memorial Building, Queen's Road, BS8 1RJ, UK.
(3) Ashima Research, 600 S. Lake Ave., Suite 104, Pasadena, CA 91106, USA.

Abstract

The orientations of aeolian features on Mars such as dunes and yardangs are controlled by the prevailing wind regime over their respective intervals of formation. Statistical analysis of the orientations of young features allows probing of Mars' recent wind regime and comparison with wind fields predicted by general circulation models (GCMs). We collect statistical distributions of transverse dune trends and yardang azimuths at nine sites on Mars (Fig. 1), and compare measured feature orientations to those predicted from interpretation of time-integrated wind vectors from the MarsWRF GCM [1, 2]. We focus on features atop interior layered deposits (ILDs) because their young surface ages [3] and erodible nature makes them applicable to determination of Mars' modern wind regime.

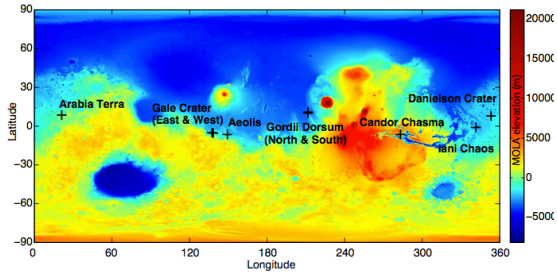

Figure 1. Location of sites selected for this study. Reference map is MOLA 32ppd topography [4].

1. Methods

1.1 Measurement of feature orientation

Dunes: Dune orientation was determined by measurement of the trend line parallel to the mean azimuth of each dune crest. Dune slip-face normals were perpendicular to this, but for transverse dunes wind direction remains 180° ambiguous. **Yardangs:** In most sites yardangs showed a distinctive teardrop shape, allowing inference of a unique wind direction. In some sites, yardangs with more elongate and parallel topography allowed inference only of a 180° ambiguous trend line.

1.2 Crater dating of interior layered deposits

To constrain the maximum age of the least transient aeolian features on ILDs we fit crater size frequency distributions measured using HiRISE images to model surface ages. We use isochrons derived by [5], which represent a refinement and synthesis of crater-dating techniques, including a correction applied to account for the loss of small (D < 20 m) bolides in Mars' atmosphere [6]. Six sites harboured sufficient crater populations to enable dating: Aeolis, Candor Chasma, Danielson Crater, Gale Crater (east), Gordii Dorsum (south) and Iani Chaos. Derived ages for most ILDs generally range between 0.1—10Ma, which agrees well with other estimates [5, 6]. ILD surfaces and aeolian features would have been subject to climate changes invoked by obliquity cycles, which occur on 4—5Ma timescales.

1.3 MarsWRF GCM sampling and prediction of feature orientation

At each site we sampled the MarsWRF GCM [1,2] for each minute of a Mars year, giving a total of 963360 wind vectors, spread uniformly throughout the year.

Transverse dune crests developed by a temporally dynamic wind field tend not to align normal or parallel to the direction of sediment transport, but to trend such that the maximum gross bedform-normal transport (GBNT) is achieved [7]. We use a modified version of [7]'s original approach, using the Fryberger flux [8] to determine the transport, and incorporating a wind stress threshold required to initiate saltation. To explore sensitivity to saltation threshold, we calculated predicted dune crest line orientations for: zero stress threshold $\sigma_t = 0$ Nm^{-2} (solid red line upper

panel in Fig. 2) a moderate stress threshold σ_t = 0.008 Nm^{-2} (dashed line) and a higher threshold σ_t = 0.016 Nm^{-2} (dotted line).

We calculate angular histograms of GCM wind vector direction (middle lower panel), with zero weighting (solid black line), weighted by mean wind stress (dashed black line), weighted by Fryberger flux with increasing saltation thresholds (green, blue and red lines) and weighted by wind stress to the fifth power (magenta line). Primary and secondary directional maxima in these distributions may correlate with, and therefore are numbered on rose diagrams of, yardang orientations (middle upper panel).

2. Example results: Gale crater (east and west sites)

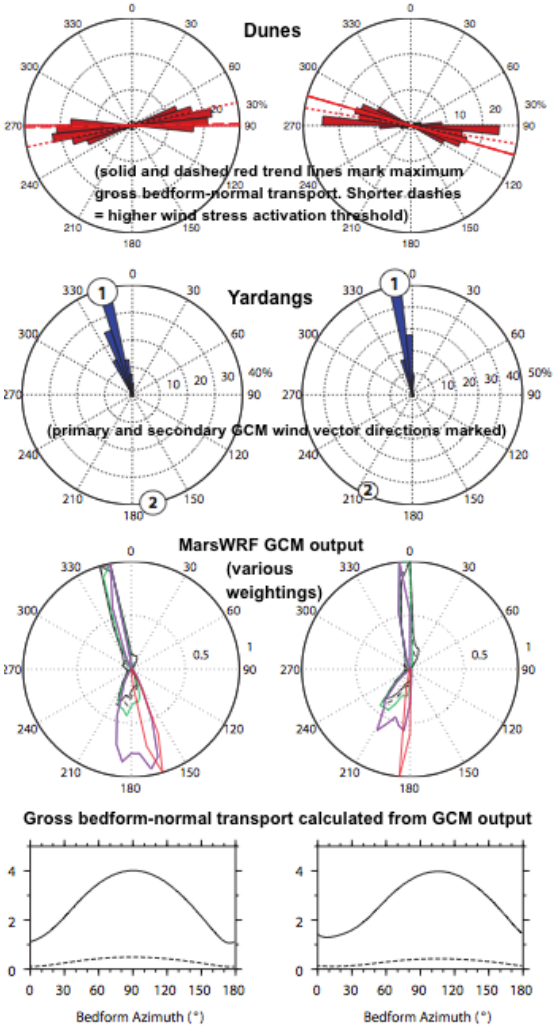

Figure 2. Comparison of aeolian features and GCM output at east and west sites in Gale Crater. Top: Dune crest orientation and GBNT. Upper middle: Yardang long axis orientation and primary wind vector direction from GCM output. Lower middle: Direction distribution of MarsWRF GCM wind vectors over one year with various weightings. Lower: GBNT calculated from from MarsWRF GCM wind vectors over all possible trends (≤ 180°).

3. Conclusions

1) In 4 out of 7 sites that had dunes, dune orientations are predicted within ~10° by the MarsWRF GCM by maximizing gross bedform-normal transport. Locations that do not match often show non-unidirectional wind fields or topographic variation. **2)** Use of higher stress thresholds (0.016 Nm^{-2}) produces better fits for dune populations at a number of locations, constraining the activation energy required for saltation. **3)** Areas where features do not match GCM output are often more topographically variable (Candor Chasma, Iani Chaos) suggesting that the MarsWRF GCM is unable to resolve localized topographic wind forcing at these small scales. **4)** Yardang populations approximately match the maximum GCM vector frequency at most sites, but at some they match secondary and tertiary directions, indicating the need for better understanding of the relationship between yardang erosion and wind fields. **5)** Slight offsets between observed and predicted yardang orientations, coupled with matches between observed and predicted dune orientations may indicate that yardangs are less in equilibrium with present day dune and wind fields (if dunes are active).

References

[1] Richardson, M. I. et al. (2007) J. Geophys. Res. 112 (E9).
[2] Toigo, A. D. et al. (2012) Icarus 221 (1), 276-288.
[3] Warner, N. H. et al. (2011) J. Geophys. Res. Plan. 116 (E06003), 1-29.
[4] Zuber, M. T., et al. (1992) J. Geophys. Res. 97 (E5), 7781-7797.
[5] Hartmann, W. K. (2005) Icarus 174, 294-320.
[6] Popova, O. et al. (2003) Met. Plan. Sci. 38 (6), 905-925.
[7] Rubin, D. M. & Hunter, R. E. (1987) Science 237, 276–278.
[8] Fryberger, S. G., 1979. In: McKee, E. D. (Ed.), U.S. G.S. Profile Pap. 1052, Washington, pp. 137–169.